Applied Catalysis B: Environmental 198 (2016) 243–253

Contents lists available at ScienceDirect

Applied Catalysis B: Environmental

journal homepage: www.elsevier.com/locate/apcatb

Photocatalytic properties of TiO_2: Effect of niobium and oxygen activity on partial water oxidation

Wenxian Li[a], Tadeusz Bak[a], Armand Atanacio[b], Janusz Nowotny[a,*]

[a] Solar Energy Technologies, Western Sydney University, Penrith, NSW 2751, Australia
[b] Australian Nuclear Science and Technology Organisation, Kirrawee, NSW 2232, Australia

ARTICLE INFO

Article history:
Received 9 March 2016
Received in revised form 20 April 2016
Accepted 20 May 2016
Available online 20 May 2016

Keywords:
Solar energy
Defect chemistry
Oxide semiconductors

ABSTRACT

This work reports the effect of niobium (0–1 at%) on photocatalytic activity and the band gap of TiO_2 with controlled oxygen activity in the range 10^{-12} Pa < $p(O_2)$ < 10^5 Pa. It is shown that maximum of photocatalytic performance in partial water oxidation is observed for Nb-doped TiO_2 containing 1 at% Nb that is processed at 1273 K in pure oxygen, $p(O_2) = 10^5$ Pa. The mechanism of photocatalytic water oxidation is considered in terms of a predominant effect of photocatalytically active surface sites corresponding to titanium vacancies. It is shown that the niobium-induced increase of the band gap, surface potential and charge transport have a minor influence on photoreactivity of Nb-doped TiO_2 with water.

1. Introduction

Titanium dioxide, TiO_2, and its solid solutions are promising candidates for solar-to-chemical energy conversion in partial and total water oxidation [1–3]. The related applied aspects involve photocatalytic water purification and the generation of solar hydrogen fuel, respectively. So far, the main research strategy in processing TiO_2 with enhanced performance in both applications is based on reduction of the band gap leading, in consequence, to increased light absorption [1–10].

Awareness is growing that band gap reduction is not always the most critical property in photocatalytic performance of oxide semiconductors, such as TiO_2 [11]. According to Lee et al. [11] the formation of nanostructured TiO_2 leads to enhanced photocatalytic activity even if its bandgap is increased. Recent study of the authors reveals that the photocatalytic performance of pure TiO_2 is determined by the concentration of defect-related surface active sites rather than the bandgap [12]. It has been shown that solar-to-chemical energy conversion should be considered in terms of a range of defect-dependent key performance-related properties, KPPs, such as charge transport, Fermi level and the concentration of surface active sites, in addition to the band gap [12–14].

1.1. Concentration of surface active sites

It has been documented that titanium vacancies are the active surface sites for water oxidation [13,14]. Recent studies show that the increase in the concentration of these sites results in an enhanced photocatalytic performance that is related to partial water oxidation [12].

1.2. Surface potential

Water oxidation is associated with removal of an electron from the adsorbed water molecule. The ability of TiO_2 to remove electrons from adsorbed species is favored by the decrease of the Fermi level in the surface layer.

1.3. Charge transport

Efficient charge transport is essential for relocation of electronic charge carriers from the site of their generation to reaction sites. Recent studies have shown that this KPP has a minor effect on the performance [12].

1.4. Band gap

Efficient light absorption by TiO_2 requires that the band gap of TiO_2 is reduced from its standard level of 3 eV and 3.2 eV for rutile and anatase, respectively. While band reduction always leads to an enhanced performance, recent studies show that reduction of band

* Corresponding author.
E-mail address: J.Nowotny@westernsydney.edu.au (J. Nowotny).

http://dx.doi.org/10.1016/j.apcatb.2016.05.044
0926-3373/

gap has a minor effect on the performance when other KPPs are not optimized [12].

1.5. Flat band potential

The flat band potential (FBP) is the external potential that is needed to compensate the internal surface potential that is responsible for band bending. The FBP, which has an effect on separation of light-induced charge carriers, may be modified by imposition of segregation- or diffusion-induced concentration gradients of charged species [12].

It has been documented that all these KPPs are associated with lattice imperfections (point defects) [13,14]. Therefore, correct understanding of the effect of materials-related properties on photocatalytic performance requires to consider defect chemistry of the studied oxide systems. Moreover, the results obtained so far indicate that photocatalysts with enhanced performance may be formed by defect engineering [13].

The aim of the present work is to verify the effect of niobium on the performance of TiO_2 in terms of the KPPs. The experimental part of the present work is preceded by the definition of terms and a brief overview of literature data on the effect of niobium on the properties of TiO_2, including photocatalytic properties.

2. Definition of terms

2.1. Defect disorder

The aim of this section is definition of the basic terms used in the present work, particularly defect chemistry of TiO_2 and its solid solutions with niobium, as well as the associated semiconducting properties.

Point defects in TiO_2, leading to nostoichiometry, are mainly formed at the gas/solid interface for the TiO_2/O_2 system. The reactions between the TiO_2 lattice and oxygen are represented by defect Equilibria (A)–(E) in Table 1 [13].

It is important to note here, that the lattice charge neutrality conditions and the $\partial \log n/\partial \log p(O_2)$ ratios in Table 1, are valid only within narrow oxygen activity regimes in which the respective defect reactions play a dominant role.

As seen, the defect Equilibria (A)-(D) involve oxygen activity, $p(O_2)$, and the concentration of electrons as parameters. Therefore, defect disorder models can be considered in terms of the effect of oxygen activity on the concentration of electrons:

$$\frac{1}{m} = \frac{\partial \log n}{\partial \log p(O_2)} \tag{1}$$

where m is the parameter. Assuming that the mobility term of electrons is independent of oxygen activity, the parameter m may be determined experimentally by the measurements of the electrical conductivity, σ, as a function of oxygen activity:

$$\frac{1}{m} = \frac{\partial \log \sigma}{\partial \log p(O_2)} \tag{2}$$

The concentration of electronic charge carriers, which is governed by intrinsic electronic equilibrium, is described by Eq. (E) in Table 1.

The incorporation of niobium into the TiO_2 lattice, leading to the formation of donor-type energy levels, is profoundly influenced by oxygen activity. The incorporation of niobium into the titanium sub-lattice of TiO_2 in reducing conditions results in the formation of electrons and gaseous oxygen [13]:

$$Nb_2O_5 \rightarrow 2Nb_{Ti}^{\bullet} + 2e' + 4O_o^{\times} + \frac{1}{2}O_2 \tag{3}$$

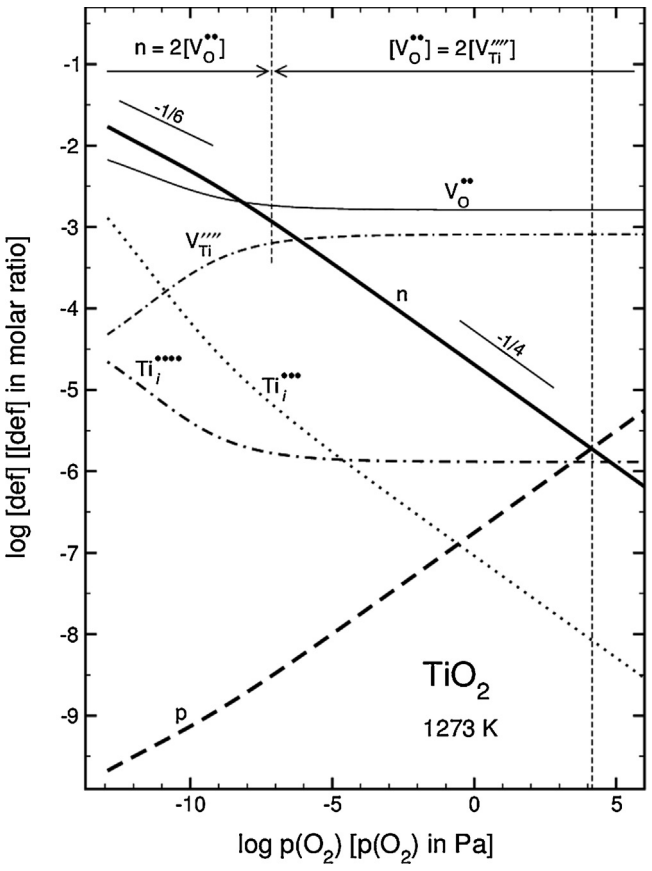

Fig. 1. Effect of oxygen activity on the concentration of intrinsic defects in TiO_2 at 1273 K [13].

However, the incorporation of niobium in oxidizing conditions results in the formation of titanium vacancies:

$$2Nb_2O_5 \rightarrow 4Nb_{Ti}^{\bullet} + V_{Ti}^{''''} + 10_o^{\times} \tag{4}$$

As a consequence, the Equilibria (3) and (4) are governed by the following respective simplified charge neutrality conditions:

$$n = \left[Nb_{Ti}^{\bullet}\right] \tag{5}$$

$$4\left[V_{Ti}^{''''}\right] = \left[Nb_{Ti}^{\bullet}\right] \tag{6}$$

The condition (5) that prevails in reducing conditions, results in a substantial increase in electrical conductivity.

The full charge neutrality for Nb-doped TiO_2 requires that:

$$4\left[V_{Ti}^{''''}\right] + \left[A'\right] + n = \left[Nb_{Ti}^{\bullet}\right] + 2\left[V_o^{\bullet\bullet}\right] + 3\left[Ti_i^{\bullet\bullet\bullet}\right] + 4\left[Ti_i^{\bullet\bullet\bullet\bullet}\right] + p \tag{7}$$

where [A'] represents the concentration of singly ionized acceptor-type impurities.

Combination of the condition (7) and the equilibria (A)–(E) in Table 1 may be used to derive the dependences between the concentration of the intrinsic defects and oxygen activity. Assuming that both donors and acceptors are present at negligibly low level, the defect disorder of TiO_2 at 1273 K may be represented by the diagram shown in Fig. 1 [13,14].

2.2. Photocatalytic properties

Photocatalytic performance of TiO_2, leading to water purification, consists in partial water oxidation resulting in the formation of active radicals that react with organic species in water, such as microbial species. The mechanism of light-induced partial water

Table 1
Basic defect equilibria in TiO_2, the associated charge neutralities and the related slope of ∂ log n versus ∂log $p(O_2)$, represented by the Kroger-Vink notation [15], where n and p denotes the concentration of electrons and electron holes, square brackets denote concentrations, and ΔH^o and ΔS^o are the enthalpy and entropy terms.

#	Defect reaction	Equilibrium Constant	Charge Neutrality	$\frac{\partial \log n}{\partial \log p(O_2)}$	ΔH^o [kJ/mol]	ΔS^o [J/(mol K)]
A	$O_O^x \Leftrightarrow V_O^{\bullet\bullet} + 2e' + \frac{1}{2}O_2$	$K_1 = \left[V_O^{\bullet\bullet}\right] n^2 p(O_2)^{1/2}$	$n = 2\left[V_O^{\bullet\bullet}\right]$	$-1/6$	493.1	106.5
B	$Ti_{Ti}^x + 2O_O^x \Leftrightarrow Ti_i^{\bullet\bullet\bullet} + 3e' + O_2$	$K_2 = \left[Ti_i^{\bullet\bullet\bullet}\right] n^3 p(O_2)$	$n = 3\left[Ti_i^{\bullet\bullet\bullet}\right]$	$-1/4$	879.2	190.8
C	$Ti_{Ti}^x + 2O_O^x \Leftrightarrow Ti_i^{\bullet\bullet\bullet\bullet} + 4e' + O_2$	$K_3 = \left[Ti_i^{\bullet\bullet\bullet\bullet}\right] n^4 p(O_2)$	$n = 4\left[Ti_i^{\bullet\bullet\bullet\bullet}\right]$	$-1/5$	1025.8	238.3
D	$O_2 \Leftrightarrow V_{Ti}^{''''} + 4h^{\bullet} + 2O_O^x$	$K_4 = \left[V_{Ti}^{''''}\right] p^4 p(O_2)^{-1}$	$p = 4\left[V_{Ti}^{''''}\right]$	$-\frac{1}{5}$	354.5	−202.1
E	nil $\Leftrightarrow e' + h^{\bullet}$	$K_i = np$	$n = p$	0	222.1	−44.6
	$\mathbf{I}nK = \left[\left(\Delta \mathbf{S^o}\right)/\mathbf{R}\right] - \left[\left(\Delta \mathbf{H^o}\right)/\mathbf{R}T\right]$					

oxidation involves a chain of reactions taking place at both anodic and cathodic sites [1–13].

The basic light-induced reaction involves ionization over the band gap leading to the formation of electron and electron hole pair, which is similar to the Reaction (E) in Table 1. In principle, the latter reaction concerns the thermodynamic equilibrium. On the other hand, however, the light-induced ionization over the band gap is a non-equilibrium process.

The formed electronic charge carriers are then separated in an electric field at the TiO_2–water interface, and transported to the anodic and cathodic active sites at the surface. The primary anodic reaction is water oxidation leading to the formation of hydroxyl species:

$$H_2O + h^{\bullet} \rightarrow HO^* + H^+ \quad (8)$$

The anodic Reaction (8), associated with removal of electron holes from the oxide surface and building-up a negative surface charge, is compensated by the cathodic reaction of TiO_2 with oxygen dissolved in water leading to creation of superoxide species:

$$O_2 + e' \rightarrow O_2^- \quad (9)$$

The formed radical species are involved in subsequent reactions, such as the formation of hydrogen peroxide through either cathodic or anodic reactions, which are represented by the following equilibria, respectively:

$$2H^+ + O_2^- + e' \rightarrow H_2O_2 \quad (10)$$

$$2H_2O + 2h^{\bullet} \rightarrow H_2O_2 + 2H^+ \quad (11)$$

The charge transfer related to the anodic Reactions (8) and (11), which require removal of electron holes from the oxide surface, is enhanced when reacting water molecule is adsorbed on the electropositive surface sites, such as titanium vacancies. On the other hand, the cathodic Reactions (9) and (10), are facilitated by electronegative sites, such as niobium ions.

3. Brief literature overview

The processing of TiO_2-based materials with enhanced photocatalytic performance in water purification is the subject of an intensive research. The most common approach in processing TiO_2-based semiconductors with enhanced solar energy conversion is reduction of the band gap [1–10]. This approach, based on the assumption that the amount of light absorption is critical for the performance in energy conversion, is correct. However, recent studies indicate that the solar-to-chemical energy conversion must be considered in terms of a wide range of properties, involving the electronic structure and the related semiconducting properties as well as the reactivity at the water/oxide interface and the associated charge transfer [11–14].

Concerning the analysis of data for Nb-doped TiO_2 the essential property is the solubility limit of Nb_2O_5 in TiO_2, which varies between 8 at% at 1173 K and >15 at% at 1973 K [13,16,17]. Only the systems within the solubility limit, forming solid solutions, are well-defined. The system involving niobium in excess of the solubility limit exhibits complex surface properties and the related data are not compatible.

Stengl et al. [18] and Joshi et al. [19] observed that the incorporation of niobium (up to 12 at%) results in an increased photocatalytic performance. Surprisingly, however, the incorporation of tantalum, which also forms donors in the TiO_2 lattice, leads to deterioration in photocatalytic performance [19].

It has been observed that heavy doping of TiO_2 with niobium results in deteriorating performance, which is considered in terms of either degeneration of semiconducting properties [20] or the formation of NbO clusters on the surface of TiO_2 [21]. On the other hand, low level doping of TiO_2, at the concentration of 0.1 at% Nb, results in a strong and stable water splitting [22].

While niobium is commonly recognized as a donor in the TiO_2 lattice, Nikolay et al. [23] observed that niobium at low concentrations leads to a decrease of the Fermi level of nano-size TiO_2, as it is observed for acceptors. This effect is explained in terms of the effect of niobium on oxygen adsorption.

The effect of niobium on surface and bulk properties of TiO_2 may differ as a result of segregation [24,25]. It has been shown that the surface concentration of niobium in Nb-doped TiO_2 annealed in oxidizing conditions is substantially larger than that in the bulk phase [25]. Moreover, segregation results in the formation of low-dimensional surface structures that are not stable in the bulk phase [25].

Mattsson et al. [26] reported that while niobium incorporation into the TiO_2 results in an enhanced light absorption, the Nb-doped TiO_2 exhibits reduced photocatalytic performance as indicated by the decomposition rate of aceton. This observation may serve as an evidence that band gap reduction is not the key property that is controlling the photocatalytic performance of TiO_2.

The flat band potential of TiO_2 and its solid solutions is profoundly influenced by the segregation-induced concentration gradients within the surface layer and the potential drop across these gradients. The surface layer of pure TiO_2 is enriched in donor-type defects, such as oxygen vacancies and titanium interstitials [12]. The related potential barrier retards the transport of electron holes to the surface. In analogy, segregation of niobium in Nb-doped TiO_2 leads to imposition of a potential barrier that prevents the transport of electron holes from the inner layers to surface anodic sites [12].

4. Postulation of the problem

In the recent work we have documented that photocatalytic performance of pure TiO_2 in oxidation of methylene blue (MB) is determined by a combined effect of the concentration of surface active sites (titanium vacancies) and surface potential, rather than the bandgap [12]. However, the established effects do not allow to distinguish which property of the two is the dominant one. The obtained data indicate that the established effect of band gap reduc-

tion does not play a major role in the performance of the studied specimens. The mechanism of the photocatalytic performance is complex and depends on a range of properties, including the electronic structure, the related semiconducting properties and surface properties.

The primary aim of this work is to verify the results obtained for pure TiO_2 [12]. Therefore, the present work involves the determination of photocatalytic properties for a similar TiO_2–based system, involving its solid solutions with niobium. While the literature overview indicates that in most cases the addition of niobium results in an enhanced photocatalytic performance, the related effects depend on concentrations and processing conditions.

The present work aims at the determination of photocatalytic performance for Nb-doped TiO_2 involving two concentrations of nibium (0.1 at% and 1 at%). The effect of niobium will be studied for the specimens annealed in a range of oxygen activities. The obtained results will be considered in terms of the same four KPPs, including surface active sites, surface potential, charge transport and the band gap.

Niobium was selected in the modification of properties of TiO_2 for the following reasons:

- The effect of niobium on defect disorder is relatively well-known
- The effect of oxygen activity on the mechanism of niobium incorporation is well-defined
- The effect of niobium on charge transport is well known
- Niobium is a good candidate in the determination of the effects of KPPs on photocatalytic performance because of its substantial effect on the concentration of surface active sites (titanium vacancies)

5. Experimental

5.1. Specimen

The specimens were obtained by solid-state reactions between pure TiO_2 and $NbCl_5$ at elevated temperatures. The basic specimen of undoped polycrystalline TiO_2 was provided by Ishihara Sangyo Kaisha (grain size 200–400 nm). Main impurities: Ca 75 ppm, Mn 12 ppm, Fe 77 ppm, Ni 15 ppm and Cu 31 ppm.

The dopant-involving compound, $NbCl_5$, was dissolved in ethyl alcohol and mixed with the TiO_2 powder at intended concentration of 0.1 and 1 at% Nb in TiO_2. The formed slurry was stirred for 10 h, dried in vacuum chamber at 333 K for 48 h in order to remove alcohol. The dry powder, with added paraffin binder (3%), was pressed into 2 mm thick pellets in a die of 13 mm of diameter under the pressure of 2 tones. The pellets were initially heated in air for 10 h at 873 K in order to remove the paraffin binder and subsequently annealed at 1273 K for 3 h in the gas flow mixture of controlled oxygen activity. Then the pellets were cooled to room temperature in the same gas phase composition.

The specimens were annealed in the tube furnace connected to the gas flow system imposing the gas flow through the reactor with the flow rate of 100 ml/min of the following compositions:

1. Pure oxygen at atmospheric pressure, $p(O_2) = 100$ kPa.
2. Argon/oxygen mixture (artificial air), $p(O_2) = 21$ kPa.
3. Pure argon. Its intrinsic oxygen activity, present as an impurity, is 10 Pa.
4. Ar/H_2 (1%) mixture. Its oxygen activity at 1273 K is $p(O_2) = 10^{-12}$ Pa.
5. Environmental (humid) air. In addition to oxygen, $p(O_2) = 21$ kPa, and nitrogen the gas involves water vapour. Assuming that the air humidity is 50%, the partial pressure of water vapour at 20 °C is approximately $p(H_2O) = 1.65$ kPa.

5.2. Band gap

The band gap was determined using Agilent Cary 5000 UV–vis-NIR spectrophotometer fitted with a 150 mm diameter integrating sphere in the external diffuse reflectance accessory (DRA-2500). The spectrophotometer was warmed-up for 30 min before calibration and the measurements. The baseline of the spectrophotometer was calibrated with standard Spectralon plates. The studied specimens were attached on the sample port for collection of the reflectance signals in the wavelength range 200–800 nm (the scanning rate was 600 nm/min). Using the Tauc model, [27,28] the band gap of the TiO_2 specimens was determined with the following expression for direct and indirect transitions:

$$[F(R_\infty)h\nu]^2 = A(h\nu - E_g) \quad (12)$$

$$[F(R_\infty)h\nu]^{1/2} = A(h\nu - E_g) \quad (13)$$

where $F(R_\infty)$ is the Kubelka-Munk function, h is the Planck constant, ν is the light frequency, A is the parameter and E_g is the band gap.

5.3. Photocatalytic performance

The light-induced effects were determined using Oriel Sol3A solar simulator, model 94043A, with 450 W lamp. The light delivered by this facility (class AAA) closely matches solar spectrum (spectral match better than 98.75%) with intensity of 1 sun at the working distance of 10 cm. The photocatalytic performance was determined by oxidation of aqueous solutions of methylene blue, MB. For the measurements, the specimens were immersed in a 10 mL of MB solution on a Teflon support. The liquid was mixed with magnetic stirrer (located under the support) in order to make the solution homogeneous. The whole system was kept in dark for two hours in order to establish the baseline absorption of MB, starting from the initial concentration of 0.01 mmol/L. Then the solar simulator was turn on to start the light-induced MB oxidation. The specimens of the MB solution were taken every 15 min to determine the concentration and then returned back to the beaker so the total solution volume remained unchanged. The changes in the MB concentration were determined spectrophotometrically by comparing the height of the absorbance peak at 670 nm.

5.4. General characterization

The general characterization of the specimens of Nb-doped TiO_2 included the SEM, visible light observation and contact angle measurements.

5.4.1. Scanning electron micrographs

The SEM micrographs of the studied specimens, including pure and Nb-doped TiO_2 annealed in the gas phases of different oxygen activities, are shown in Fig. 2.

As seen, the morphology of the specimens, which depends on the content of niobium and oxygen activity, may be summarized in the following points:

1. *Pure TiO_2*. The grain size of pure TiO_2 in oxidizing conditions [10 Pa $< p(O_2) < 10^5$ Pa] is practically independent of oxygen activity (200–400 nm), except the specimen annealed in artificial air (~500 nm). The annealing results in sintering of the ceramic body leading to the formation of necks between grains. Annealing in strongly reducing conditions results in large grain growth to the size of 600–800 nm.
2. *Nb-Doped TiO_2*. The morphology of Nb-doped TiO_2 is similar of that of pure TiO_2, however, the sintering process is less advanced and necks are less developed. The specimens

annealed in strongly reducing conditions have the grain size of 600–800 nm.

3. *Grain Growth*. The observed grain growth in strongly reducing conditions is consistent with the enhanced mass transport due to the increased concentration of highly mobile defects; oxygen vacancies and titanium interstitials as represented by the defect disorder diagram (Fig. 1).

5.4.2. Optical photographs

The visible light images reflecting the effect of the annealing conditions on colours are shown in Fig. 3.

As seen, the samples reduced in the Ar-H_2 mixture are black for pure TiO_2 as well as for Nb-doped TiO_2. The Nb-doped TiO_2 annealed in Ar shows slight gray color. The remaining specimens are sandy-white independently of the annealing conditions and niobium contents.

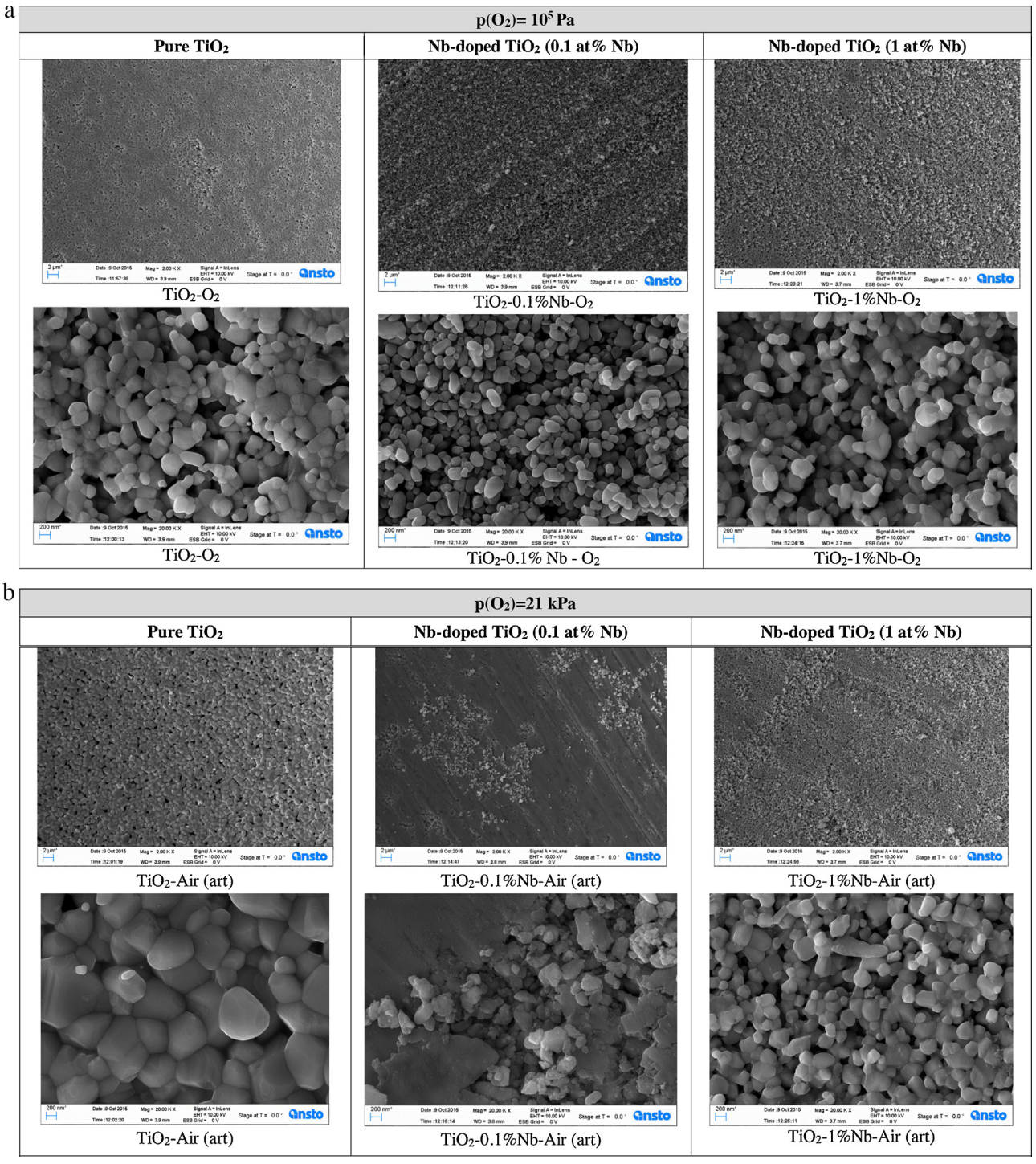

Fig. 2. (a) The SEM micrographs of the studied specimens including pure and Nb-doped TiO_2 annealed in pure oxygen. $p(O_2) = 10^5$ Pa. (b) The SEM micrographs of the studied specimens including pure and Nb-doped TiO2 annealed in artificial air, p(O2) = 21 kPa. (c) The SEM micrographs of the studied specimens including pure and Nb-doped TiO_2 annealed argon, $p(O_2) = 10$ Pa. (d) The SEM micrographs of the studied specimens including pure and Nb-doped TiO_2 annealed in the argon-hydrogen (1%) mixture, $p(O_2) = 10^{-12}$ Pa. (e) The SEM micrographs of the studied specimens including pure and Nb-doped TiO_2 annealed in atmospheric (humid) air, $p(O_2) = 21 \times 10^4$ Pa.

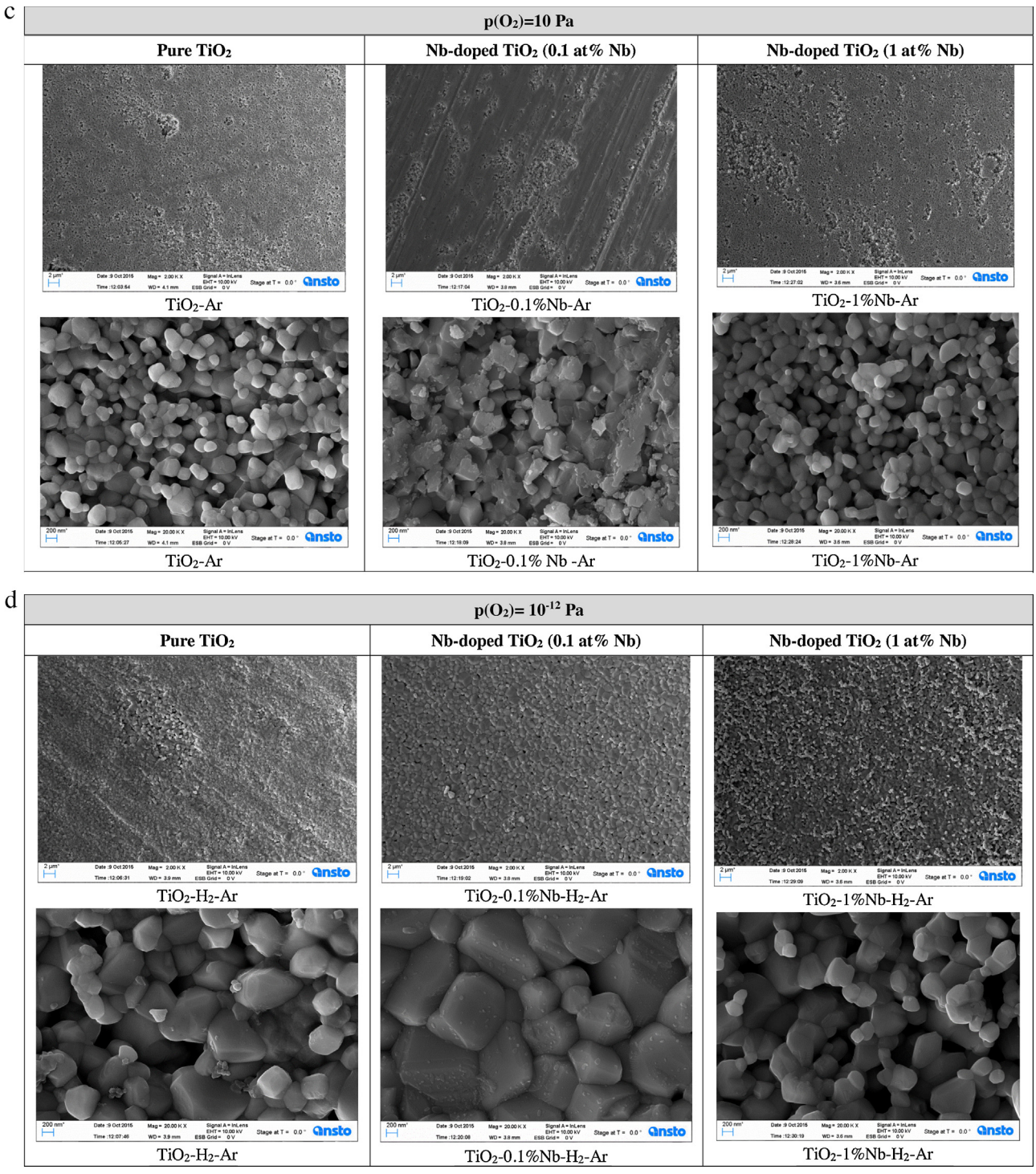

Fig. 2. (*Continued*)

5.4.3. Contact angle

The contact angle was measured for the water drop of 5 μl in weak natural light to avoid light induced water hydrophilic effect. The shapes of the water droplets are shown in Fig. 4. The resulting effect of oxygen activity and niobium composition on the determined contact angle is shown in Fig. 5.

As seen, the contact angle assumes the largest value for pure TiO_2 annealed in strongly reducing conditions imposed by the argon-hydrogen mixture. The smallest contact angle is observed for Nb-doped TiO_2 involving 1 at% Nb annealed in pure oxygen. In general, the contact angle decreases with the increase of both niobium content and oxygen activity.

6. Results and discussion

This section considers the experimental results on the effect of niobium and oxygen activity on photocatalytic activity, related to the decomposition rate of MB. The effect will be discussed in terms of the KPPs, including the surface active sites, Fermi level, charge transport and bandgap. The obtained results will be used in

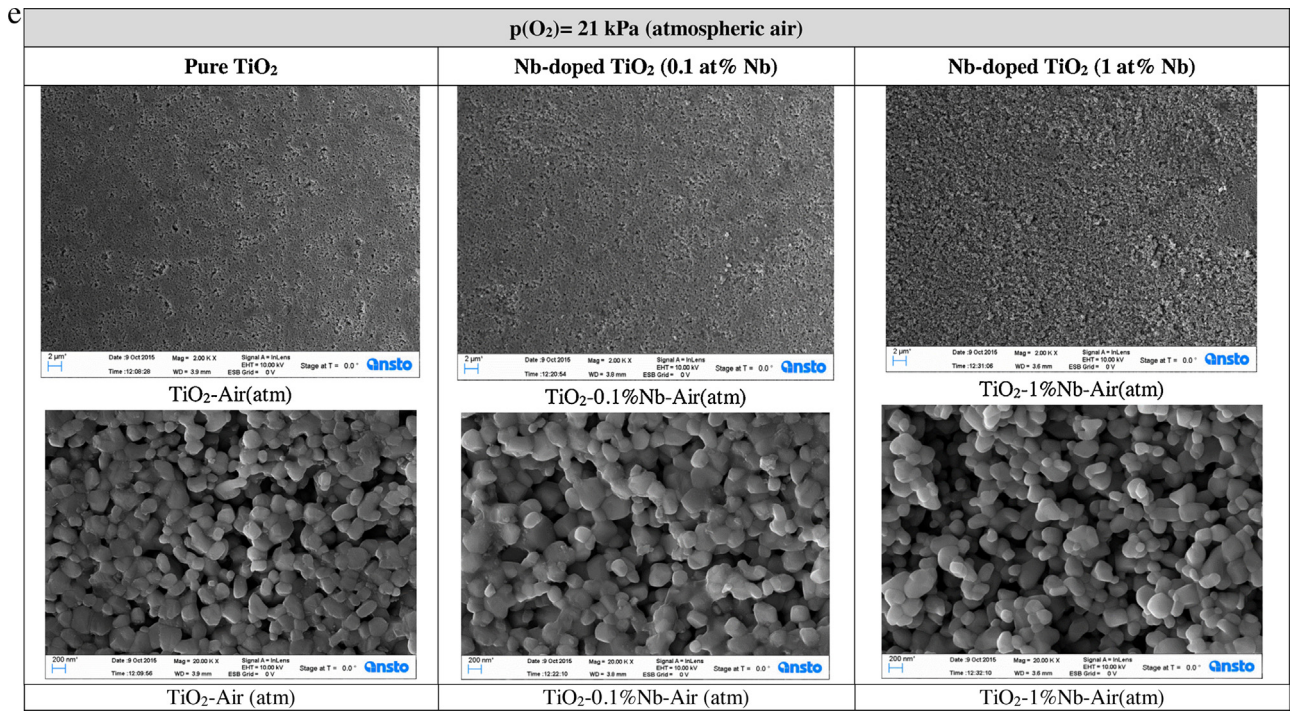

Fig. 2. (*Continued*)

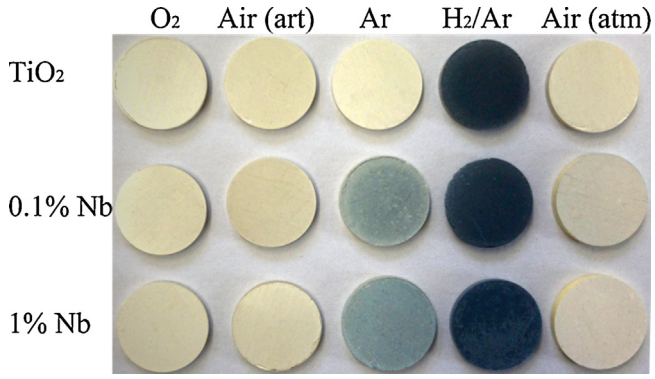

Fig. 3. The photographs of pure TiO_2, 0.1 at% Nb-doped TiO_2, and 1 at% Nb-doped TiO_2 annealed in O_2, artificial air, Ar, H_2/Ar mixture, and atmospheric air, respectively.

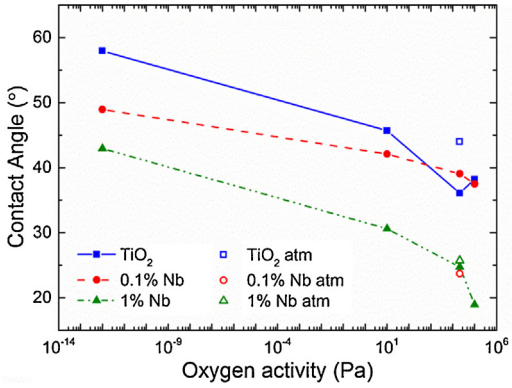

Fig. 5. The effect of oxygen activity in the gas phase during annealing on the contact angle for pure TiO_2, 0.1 at% Nb-doped TiO_2, and 1 at% Nb-doped TiO_2 (where "atm" corresponds to the atmospheric environment).

derivation of a theoretical model on the light-induced reactivity of Nb-doped TiO_2 with water and the related charge transfer.

Before reporting the data on photocatalytic properties, let us consider the effect of niobium and oxygen activity on the KPPs. The expected tendency of changes in the specific KPPs as a function of oxygen activity and the content of niobium are represented in Fig. 6 by the left and the right column, respectively.

6.1. Surface active sites

Titanium vacancies have been identified as anodic surface sites that are able to form an active complex with water molecules leading, ultimately to water oxidation [13]. Their concentration depends on oxygen activity and the concentration of niobium

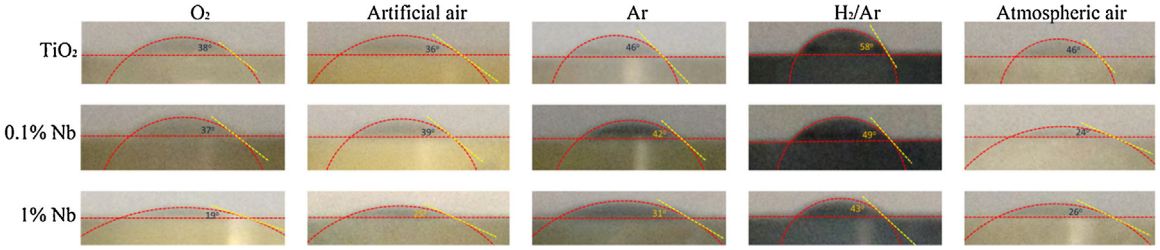

Fig. 4. The contact angle variation of pure TiO_2, 0.1 at% Nb-doped TiO_2, and 1 at% Nb-doped TiO_2 annealed in O_2, artificial air, Ar, H_2/Ar mixture, and atmospheric air, respectively.

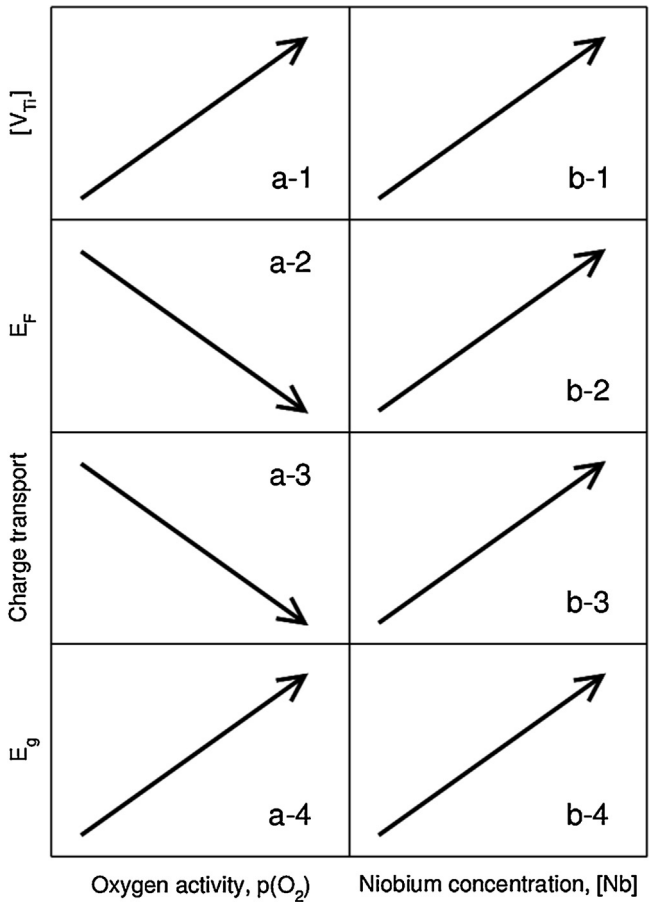

Fig. 6. Schematic representation of the expected effect of oxygen activity (left) and niobium content (right) on the KPPs, including surface active sites, [V_{Ti}], Fermi level, E_F, charge transport and bandgap, E_g.

as schematically represented in Fig. 6**a-1** and **b-1,** respectively. According to the Equilibrium (D) in Table 1, the increase of oxygen activity results in an increased concentration of titanium vacancies. The incorporation of niobium in oxidizing conditions also leads to the formation of titanium vacancies as represented by Equilibrium (4). Therefore, both higher oxygen activity and larger concentration of niobium result in an increase of the concentration of the anodic surface active sites for water oxidation.

6.2. Surface Fermi level

The Fermi level or the chemical potential of electrons is directly related to the concentration of electrons, n:

$$E_F = const + kT \ln \frac{n}{N_n} \quad (14)$$

where N_n is the density of states. As seen in the Equilibria (A)–(C) in Table 1, the concentration term n is increased when oxygen activity is reduced due to the formation of donor-type intrinsic defects, such as oxygen vacancies and titanium interstitials. Consequently, Fermi level decreases with increased oxygen activity as represented schematically in Fig. 6**a-2**. According to Equilibrium (3), the increase in the concentration of niobium in reducing conditions results in an increase in the concentration of electrons and the E_F. The incorporation of niobium in oxidizing conditions leads to the increase in the concentration of both niobium in titanium sites (donors) and titanium vacancies (acceptors). However, taking into account the difference in their ionization energies, these also leads to an increase in the Fermi level as represented in Fig. 6**b-2**.

6.3. Charge transport

The charge transport is related to the product of the concentration and mobility terms. The concentration of electrons increases with the decrease in oxygen activity due to the increase in the concentration of donors (oxygen vacancies and titanium interstitials). Also the increase in the concentration of niobium leads to an increased concentration of electrons. Therefore, assuming – in

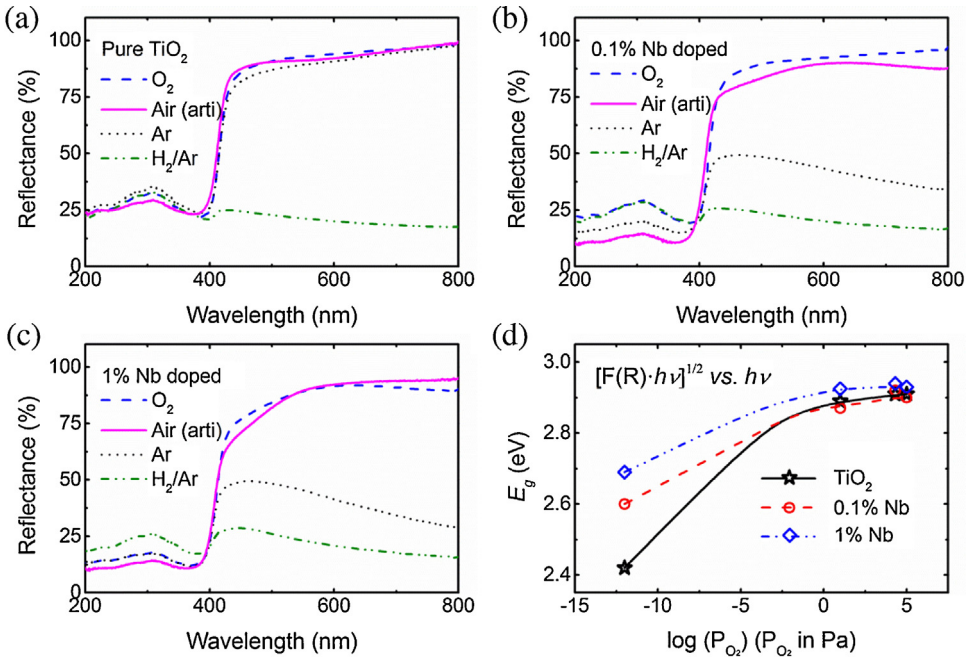

Fig. 7. The diffusion reflectance of (a) pure TiO_2, (b) 0.1 at% Nb-doped TiO_2, and (c) 1 at% Nb-doped TiO_2 annealed in O_2, artificial air, Ar, and H_2/Ar mixture, respectively. (d) The bandgap variation depending on the annealing oxygen activity derived from UV–vis reflectance using Kubelka-Munk relationship, $[F(R)h\upsilon]^{1/2}$ *vs.* $h\upsilon$ for indirect bandgap model, where $F(R) = (1-R)^2/2R$ (R is reflectance).

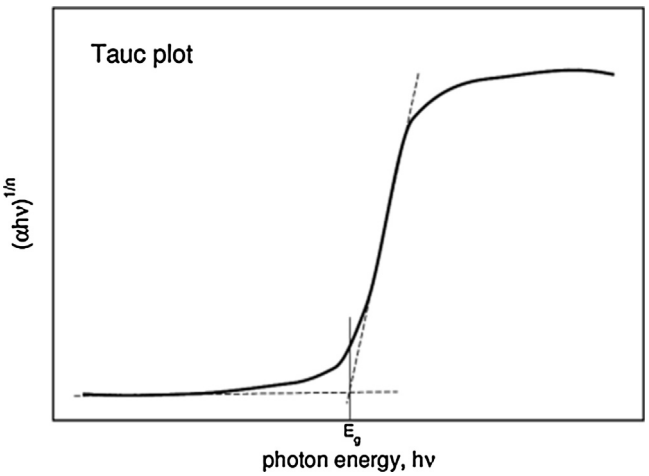

Fig. 8. Schematic representation of band gap determination.

the first approximation – that the mobility terms is independent of oxygen activity and the concentration of niobium, the charge transport decreases with increased oxygen activity (Fig. 6**a-3**) and increases with increased concentration of niobium (Fig. 6**b-3**).

6.4. Band gap

The effect of oxygen activity and niobium on the band gap was assessed by the measurements of the diffusion reflectance spectra, which are shown in Fig. 7 (a–c). The resulting band gap, determined for indirect transitions, as a function of the applied oxygen activity, is shown in Fig. 7 d.

The method of the determination of the bandgap from the diffusion reflectance is shown schematically in Fig. 8.

As seen, the onset of the reflectance spectra corresponds to ~400 nm (~3 eV) for all studied specimens. The reflectance spectra of pure TiO_2 annealed in O_2, artificial air and argon (Fig. 7**a**) show strong reflectance at E < 3 eV and sudden increase of absorbance at band gap energy (E > 3 eV). On the other hand, the observed weak reflectance for pure TiO_2 annealed in the Ar/H_2 mixture, across the entire energy range, both below and above the band gap energy, can be considered in terms of the effect of high concentration of oxygen vacancies and interstitial titanium ions. These defects, which introduce large number of additional energy levels within the band gap, are responsible for high light absorption within the band gap energy range.

Table 2
The effect of oxygen activity on the bandgap of the studied specimens (in eV).

Specimens	Oxygen Activity				
	100 kPa	21 kPa	10 Pa	10^{-12} Pa	21 kPa (air)
Pure TiO_2	2.91	2.91	2.89	2.42	2.89
Nb-TiO_2 (0.1 at%)	2.9	2.92	2.87	2.6	2.94
Nb-TiO_2 (1 at%)	2.93	2.94	2.925	2.69	2.94

As seen in Fig. 7**b** and **c**, the spectra for Nb-doped TiO_2 exhibit strong sub-bandgap reflectance for the specimens annealed in oxygen and air, however, the light absorption of the specimens reduced in argon and the hydrogen-argon mixture is much stronger. The observed effect of oxygen activity on reflectance seems to be related the effect of oxygen activity on the extent of niobium segregation. The strong bandgap reflectance in oxidizing conditions, corresponding to high surface concentration of niobium, seems to be affected by low concentration of oxygen vacancies, which are responsible for absorption.

The combined effect of both oxygen activity and niobium on the band gap is represented in Fig. 7**d** and Table 2. As seen, the decrease of oxygen activity results in reduction of the band gap, however, the effect of the bandgap reduction is diminished by the increased concentration of niobium. The effect of oxygen activity and the concentration of niobium on the band gap is represented in Figs. 6**a-4** and **b**-4.

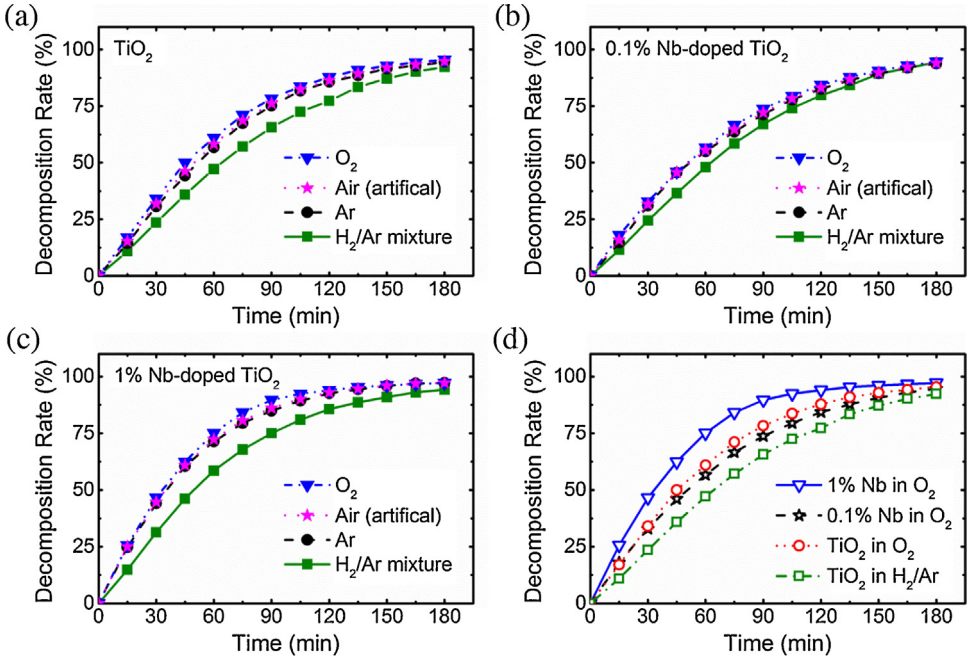

Fig. 9. The photocatalytic decomposition rate of MB as a function of reaction time for (a) pure TiO_2, (b) 0.1 at% Nb-doped TiO_2, and (c) 1 at% Nb-doped TiO_2 annealed in O_2, artificial air, Ar, and H_2/Ar mixture. (d) The comparison of the photocatalytic decomposition rate of MB using samples annealed in pure O_2 and pure TiO_2 annealed in H_2/Ar mixture. It is concluded that 1 at% Nb-doped TiO_2 annealed in pure oxygen shows the best photocatalytic performance.

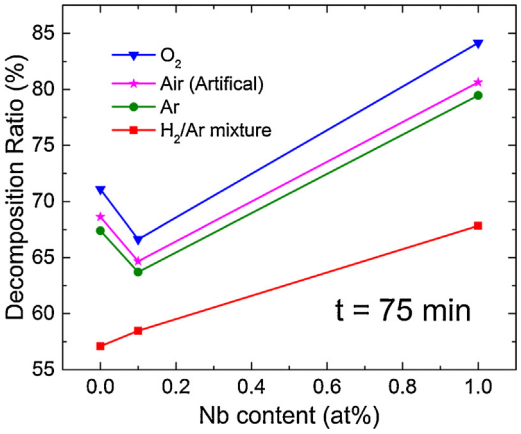

Fig. 10. Combined effect of both oxygen activity and the concentration of niobium on the photocatalytic decomposition rate at the time t = 75 min.

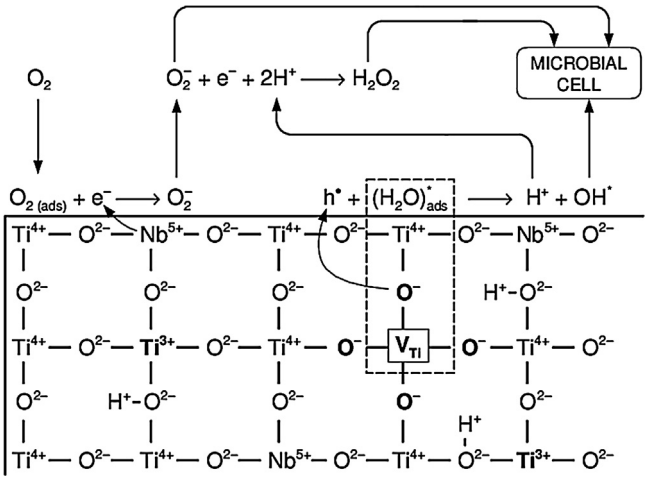

Fig. 11. Mechanism of the reactivity of Nb-doped TiO_2 with water and the related charge transfer.

6.5. Photocatalytic activity

The effect of the gas phase and the related oxygen activity during annealing of the specimens on their performance, related to photocatalytic decomposition rate of MB, is represented in Fig. 9, including pure TiO_2 (**9a**), Nb-doped TiO_2 involving 0.1 at% Nb (**9b**) and Nb-doped TiO_2 involving 1 at% Nb (**9c**). The combined effect of oxygen activity and the concentration of niobium is shown in Fig. 9**d**.

As seen, the strongest photocatalytic activity, reflected by the rate of MB decomposition rate, is observed at highest concentration of niobium and the largest oxygen activity. This behavior indicates that the KPP responsible for the performance is the concentration of the surface active sites.

The combined effect of the concentration of niobium and oxygen activity on the photocatalytic performance, related to the decomposition rate at 75 min of the experiments represented in Fig. 9 is shown in Fig. 10.

The data in Fig. 10 represent a combined effect of all KPPs on the performance. The observed effect of oxygen activity on the decomposition ratio indicates the dominant effect of the concentration of surface active sites on the performance for all specimens, including pure and Nb-doped TiO_2 as it is represented in Fig. 6**a-1**. This effect is consistent with the reaction mechanism assuming that the primary reactions of water oxidation are the anodic reactions represented by Equilibria (8) and (11). Comparison of the performance for pure TiO_2 and the Nb-doped specimen containing 1 at% Nb is consistent with this mechanism. The exceptional behavior observed for the Nb-doped TiO_2 involving 0.1 at% Nb indicates that the observed decreased photocatalytic activity in this specific case is predominantly influenced by the increased surface potential as a result of niobium doping (Fig. 6**b-2**).

The observed dependences in Fig. 10 indicate that the changes of the bandgap as a result of both oxygen activity and niobium concentration, as represented by Figs. 6**a-4** and 6**b-4**, have minor effect on the observed performance. The significance of this observation is that it indicates that the photocatalytic performance must be related to a range of KPPs, in addition to the bandgap. In other words, the present work indicates that the bandgap has little effect on the performance. This observation does not question the effect of the bandgap on photocatalytic performance. The combined effect of niobium concentration and oxygen activity on the decomposition of MB indicates, however, that the photocatalytic performance must be considered as a combined effect of all KPPs, including the concentration of surface active sites, Fermi level, charge transport and the bandgap. The effect of the latter quantity on the performance becomes more significant when the remaining KPPs are optimized and their effect is minimized.

The effect of charge transport on performance should be considered in terms of the charge displacement along and across the surface layer. In the latter case the transport is affected by the electric field generated by the segregation-induced concentration gradients.

Addition of niobium results in an increase of charge transport along the surface. The effect of this KPP is not observed at the lower concentration of niobium (0.1 at%). The enhanced performance at 1 at% Nb could be affected by the enhanced charge transport, however, the observed effect of oxygen on the decomposition rate is in conflict with this observation. Therefore, is seems that the charge transport has a minor effect on the performance, if any.

The charge transport across the surface layer of Nb-doped TiO_2 may be affected by the segregation-induced concentration gradients. One should expect that such gradients of niobium formed at high oxygen activity will retard the transport of the light-induced electron holes from inner layers towards the surface. The observed effect of niobium on the performance indicates that this kind of charge transport is affecting the performance.

The determination of the effect of segregation on the charge transport along and across the surface requires the specimens with controlled composition within the surface layer. Such studies are being in progress.

In summary, the present work confirms that the photocatalytic performance of TiO_2 should be considered in terms of a competitive effect of several KPPs. The dominant effects depend on specific surface vs. bulk compositions including oxygen activity and the concentration of extrinsic defects, such as niobium. It is essential to note that while the effect of reduced band gap of TiO_2 is not observed in this work, reduction of the band gap is always critical for enhanced light absorption and solar-to-chemical energy conversion. In order words, the effect of reduced band gap on the performance is not observed simply because the effect of other KPPs, such as the concentration of the surface active sites, in this specific circumstances is more important.

Fig. 5 represents the effect of oxygen activity on the contact angle, which is related to hydrophilicity. As seen, contact angle can be minimized by the decrease of oxygen activity and increased concentration of niobium. These results can be considered in terms of hydro-philicity and the related concentration of oxygen vacancies [29]. The vacancy concentrations are high for the samples annealed in H_2/Ar mixture, based on the defect diagram shown in Fig. 1.

The results obtained in this work may be considered in terms of the theoretical model representing mechanism of the reactivity of the TiO_2 surface with water and the related charge transfer (Fig. 11).

The reaction step of a fundamental importance is adsorption of water on the anodic active sites (titanium vacancies) leading to the formation of an active complex. Its reaction with an electron hole results in the formation of protons and hydroxyl radicals, OH^*. The fundamental cathodic reaction consists in reduction of oxygen molecule, by an electron provided by the surface donors, such as niobium ions, leading to the formation of superoxide oxygen species O_2^-. These species react with protons resulting in the formation of hydrogen peroxide, H_2O_2. All these reactive species are involved in oxidation of organic compounds present in water, such as microbial cells or MB.

7. Conclusions

The results obtained in this work indicate that Nb-doped TiO_2 is a good system for the investigation of the effect of defect disorder and the related KPPs on photocatalytic performance in the light-induced partial oxidation of water. The present work indicates that the combination of niobium content and oxygen activity allows the modification of the KPPs, such as the concentration of anodic surface active sites, Fermi level, charge transport and bandgap within a wide range. The data analysis indicates that all these KPPs have an effect on the photocatalytic performance, however, their appearance depends on both oxygen activity in the TiO_2 lattice and niobium contents, and the associated defect disorder.

The reported data suggest that the concentration of the *anodic surface active sites* have the paramount effect on performance. This has been documented by the dependence of the performance on oxygen activity for all compositions and the effect of niobium at the highest concentration. Surprisingly, the data obtained in this work strongly indicate that the *band gap*, altered by oxygen activity and niobium content, has a minor effect on performance.

The observed influence of oxygen activity on the performance is consistent with a joint contribution of the *Fermi level-related KPP* and the concentration of the surface active sites. It is difficult to assess the individual contribution of these two KPPs.

Acknowledgement

The support of the Australian Renewable Energy Agency (ARENA) through fellowships provided to WL is acknowledged.

References

[1] O. Carp, C.L. Huisman, A. Reller, Prog. Solid State Chem. 32 (2004) 33.
[2] K. Nakata, A. Fujishima, J. Photochem. Photobiol. C 13 (2012) 169.
[3] T. Ochiai, A. Fujishima, J. Photochem. Photobiol. C 13 (2012) 247.
[4] T.J. Kemp, R.A. McIntyre, Polym. Degrad. Stab. 91 (2006) 165.
[5] H. Yamashita, M. Harada, J. Misaka, M. Takeuchi, K. Ikeue, M. Anpo, J. Photochem. Photobiol. A 148 (2002) 257.
[6] O. Diwald, T.L. Thompson, E.G. Goralski, S.D. Walck, J.T. Yates, J. Phys. Chem. B 108 (2004) 52.
[7] S.U.M. Khan, M. Al-Shahry, W.B. Ingler, Science 297 (2002) 2243.
[8] S. Sakthivel, H. Kisch, Angew. Chem. Int. Ed. 42 (2003) 4908.
[9] R. Asahi, T. Morikawa, T. Ohwaki, K. Aoki, Y. Taga, Science 293 (2001) 269.
[10] X.B. Chen, L. Liu, P.Y. Yu, S.S. Mao, Science 331 (2011) 746.
[11] H.S. Lee, C.S. Woo, B.K. Youn, S.Y. Kim, S.T. Oh, Y.E. Sung, H.I. Lee, Top. Catal. 35 (2005) 255.
[12] T. Bak, J. Nowotny, N. Sucher, E. Wachsman, J. Chem. Phys. C 115 (2011) 15711.
[13] J. Nowotny, Oxide Semiconductors for Solar Energy Conversion: Titanium Dioxide, CRC Press, Boca Raton, 2012.
[14] T. Bak, W. Li, J. Nowotny, A.J. Atanacio, J. Davis, J. Chem. Phys. A 119 (2015) 9465.
[15] F.A. Kröger, H.J. Vink, Relations between the concentrations of imperfections in crystalline solids, in: S. Frederick, T. David (Eds.), Solid State Physics, vol. 3, Academic Press, 1956, pp. 307–435.
[16] N.G. Eror, J. Solid State Chem. 38 (1981) 281.
[17] A. Trenczek-Zając, M. Radecka, M. Rekas, Physica B 399 (2007) 55.
[18] V. Stengl, V. Houskova, S. Bakardjieva, N. Murafa, P. Bezdicka, J. Mater. Res. Soc. 25 (2010) 2015.
[19] B.N. Joshi, H. Yoon, M.F.A.M. van Hest, S.S. Yoon, J. Am. Ceram. Soc. 96 (2013) 2623.
[20] A.V. Emeline, Y. Furubayashi, X. Zhang, M. Jin, T. Murakami, A. Fujishima, J. Phys. Chem. B 109 (2005) 24441.
[21] J. Arbiol, J. Cerdà, G. Dezanneau, A. Cirera, F. Peiró, A. Cornet, J.R. Morante, J. Appl. Phys. 92 (2002) 853.
[22] C. Das, P. Roy, M. Yang, H. Jha, P. Schmuki, Nanoscale 3 (2011) 3094.
[23] T. Nikolay, L. Larina, O. Shevaleevskiy, B.T. Ahn, Energy Environ. Sci. 4 (2011) 1480.
[24] D. Morris, Y. Dou, J. Rebane, C.E.J. Mitchell, R.G. Egdell, D.S.L. Law, A. Vittadini, M. Casarin, Phys. Rev. B 61 (2000) 13445.
[25] A.J. Atanacio, T. Bak, J. Nowotny, J. Phys. Chem. C 118 (2014) 11174.
[26] A. Mattsson, M. Leideborg, K. Larsson, G. Westin, L. Österlund, J. Phys. Chem. B 110 (2006) 1210.
[27] J. Tauc, R. Grigorovici, A. Vancu, Physica Status Solidi (b) 15 (1966) 627.
[28] S.K. Oleary, P.K. Lim, Solid State Commun. 104 (1997) 17.
[29] A. Fujishima, X. Zhang, C.R. Chim. 9 (2006) 750.